Available on CMS information server

CMS AN -2017/056

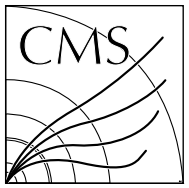

The Compact Muon Solenoid Experiment

Analysis Note

The content of this note is intended for CMS internal use and distribution only

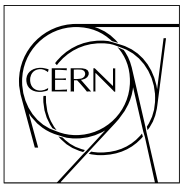

21 February 2017 (v4, 01 June 2019)

Selection for the single top t-channel analyses with the 2016 dataset at 13 TeV

T. Chwalek, A. De Iorio, N. Faltermann , A. Giammanco , Alberto Orso Maria Iorio , W.A. Khan , M. Komm , L. Lista , Th. Muller , and P. Ott,

Abstract

In the current note the basic object selection for the t-channel inclusive and differential cross section analyses at 13 TeV with the 2016 dataset is described. The targeted final state topology involves exactly one lepton (muon or electron) produced in association with 2-4 jets, 1-2 of which coming from the b-quark hadronisation. In this note we describe and motivate the physics object selection applied, the datasets and triggers used.

CMS AN-17-056

2019/02/04
Head Id: 445970
Archive Id: 488169
Archive Date: 2018/02/14
Archive Tag: trunk

Event selection for *t*-channel single-top-quark analyses with the 2016 dataset at 13 TeV

T. Chwalek[2], N. Faltermann[2], A. Giammanco[1], A. O. M. Iorio[3], W. A. Khan[3], M. Komm[1], L. Lista[3], Th. Müller[2], P. Ott[2], and T. Pambor[2]

[1] Université Catholique de Louvain, Center for Particle Physics and Phenomenology, Louvain-la-Neuve, Belgium
Fonds National de Recherche Scientifique, Belgium
[2] Institut für Experimentelle Kernphysik, Karlsruher Institut für Technologie, Germany
[3] Istituto Nazionale di Fisica Nucleare sez. Napoli, Italy

Abstract

The basic object selection for the *t*-channel inclusive and differential cross section measurements at 13 TeV with the 2016 dataset is described. The corresponding signatures involve exactly one lepton (muon or electron) produced in association with two to four jets, of which one or two stem from the hadronisation of a b quark. The used physics object selection, the datasets, the triggers, and the event reconstruction are detailed in this note.

Contents

1 Introduction

Top quarks produced singly through electroweak interactions in t-channel feature a final state that includes the top quark decay products and one or two additional jets, of which one can be b-tagged. The Feynman diagrams of t-channel single-top-quark production are reported in Fig. 1. We consider the cases where the top quark decays leptonically as $\mathrm{t} \to \mathrm{Wb} \to \ell\nu\mathrm{b}$ with $\ell = \mathrm{e}/\mu$[1]. Therefore the final state of both channels features significant missing transverse energy, exactly one charged lepton (electron or muon), and one b jet from the top quark decay. In addition the t-channel final state encompasses one light jet coming from the non-b "spectator" quark which is typically found in the forward detector region ($|\eta| \sim 3$) since it recoils against the top quark via W boson exchange. A potential second b-jet coming from gluon splitting can also be present which is however often outside the acceptance.

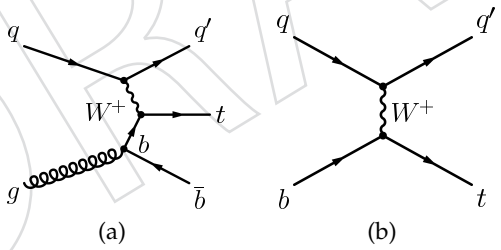

Figure 1: Leading order Feynman diagrams for single top quark production via the t-channel in the four flavour scheme (a) and in the five flavour scheme (b). (b) can also be seen as an NLO contribution in the four flavor scheme.

The aim of this note is to describe the setup of the analyses concerning the object selection, the datasets, the event reconstruction, the trigger definition, and the applied scale factors for those processes which have been synchronized amongst the involved groups.

The note is organized as follows:

- Sec. 2 introduces the samples of simulated events and the datasets;
- Sec. 3 describes the physics object and the applied event selection;

[1] Intrinsically this includes also muons or electrons from the decay of intermediate tau leptons, i.e. $\mathrm{t} \to \tau\nu_\tau\mathrm{b} \to (\ell\nu)\nu_\tau\mathrm{b}$.

- Sec. 4 details the kinematic reconstruction of top quarks under the signal hypothesis;
- Sec. 5 elaborates the trigger strategy and the determination lepton trigger, identification, and isolation efficiency corrections.

2 Samples

Signal t-channel single-top-quark events as well as $\mathrm{t\bar{t}}$ and tW background events are generated with POWHEG [1–4] (version 2 for t-ch./$\mathrm{t\bar{t}}$ and version 1 for tW). The latter is simulated in the 5FS. The value of the top-quark mass used in simulated top-quark samples is $m_{\mathrm{t}} = 172.5$ GeV. For all samples PYTHIAv8.180 [5] with tune CUETP8M1 [6] is used for the modelling of the showering. The production of W or Z bosons in association with jets is generated using aMC@NLO and the FxFx merging scheme [7], where one generates up to two additional partons at the ME level, along with PYTHIA8. QCD multijet events, generated with PYTHIAv8.180, are used to study the data-driven methods of estimating this background. All generated events undergo a full simulation of the CMS detector response. Additional proton-proton interactions (pileup) using minimum bias events are overlaid in the simulation with a similar frequency of occurrence as observed in data.

The analyses are using data and simulated events, listed in Tab 1, which are available in the official miniAOD format [8]. For data, only certified (golden) luminosity sections are selected from the datasets during which the detector was fully operational. The combined dataset corresponds to an integrated luminosity of about 35.9 fb^{-1} for electron and muon events respectively.

Simulated signal events are normalized to the NLO cross section of

$$\begin{aligned} \sigma_{t\text{-ch.,t}} &= 136.02^{+4.09}_{-2.92}\,(\text{scale}) \pm 3.52\,(\text{PDF}) \\ \sigma_{t\text{-ch.,}\bar{\mathrm{t}}} &= 80.95^{+2.53}_{-1.71}\,(\text{scale}) \pm 3.18\,(\text{PDF}) \\ \sigma_{t\text{-ch.}} &= 216.99^{+6.62}_{-4.64}\,(\text{scale}) \pm 6.16\,(\text{PDF}) \end{aligned} \quad (1)$$

evaluated in the 5FS within HATHOR v2.1 [10, 12]. Table 2b summarizes the Monte-Carlo samples for signal and backgrounds, and provides the cross section for each sample. All the cross sections have been taken from the references listed in Table 2b or, when no reference is given, from the generator itself. The simulation of the detector response is based on GEANT 4 [13] and assumes realistic alignment and calibration tuned on data.

3 Physics object selection

The final-state topology in the t-channel is characterized by the presence of exactly one isolated charged lepton and a b jet from the top quark decay, as well as a light-flavoured jet produced in the forward region. Potential gluon splitting in the initial state leads to a second b quark (Fig. 1) that recoils against the top quark and thus has generally a softer p_{T} spectrum and a broader $|\eta|$ distribution compared to the b quark produced in the top-quark decay. The acceptance of events with two b jets reconstructed in the final state is therefore expected to be small. In fact we can anticipate that using the selection described in this section, the number of signal events with two b jets reconstructed in the detector is smaller than the number of events with just one b jet. In the following, we describe the object definitions and selection criteria.

Table 1: Datasets and Monte Carlo (MC) samples used in the analyses. The MC samples are generated either inclusively or with a final state restricted to the leptonic mode, including electrons, muons, and taus. Where no references are given, the cross sections come from the generator itself. For the samples restricted to specific decay channels the branching ratio (BR) is included in the cross section value quoted. The "RunIISpring15MiniAODv2-74X_mcRun2_asymptotic_v2-v1" part in the name is the same for all samples and has been replaced by "...".

Dataset	Run range	Integrated luminosity
/SingleMuon(SingleElectron)/Run2016B-03Feb2017_ver2-v2/MINIAOD	272007-275376	5.8
/SingleMuon(SingleElectron)/Run2016C-03Feb2017-v1/MINIAOD	275657-276283	2.6
/SingleMuon(SingleElectron)/Run2016D-03Feb2017-v1/MINIAOD	276315-276811	4.2
/SingleMuon(SingleElectron)/Run2016E-03Feb2017-v1/MINIAOD	276831-277420	4.0
/SingleMuon(SingleElectron)/Run2016F-03Feb2017-v1/MINIAOD	277772-278808	3.1
/SingleMuon(SingleElectron)/Run2016G-03Feb2017-v1/MINIAOD	278820-280385	7.5
/SingleMuon(SingleElectron)/Run2016H-03Feb2017_ver2-v1/MINIAOD	280919-284044	8.6
/SingleMuon(SingleElectron)/Run2016H-03Feb2017_ver3-v1/MINIAOD		

(a) Certified (golded) data samples [9].

Process	$\sigma(\cdot BR)$[pb]	Dataset name
single top (t-ch)	136.02 (NLO) [10]	/ST_t-channel_4f_inclusiveDecays_13TeV-powhegV2-madspin-pythia8_TuneCUETP8M1/...
single antitop(t-ch)	80.95 (NLO) [10]	/ST_t-channel_4f_inclusiveDecays_13TeV-powhegV2-madspin-pythia8_TuneCUETP8M1/...
single top (tW)	35.6 (NNLL) [11]	/ST_tW_top_5f_inclusiveDecays_13TeV-powheg-pythia8_TuneCUETP8M1/...
single anti-top (tW)	35.6 (NNLL) [11]	/ST_tW_antitop_5f_inclusiveDecays_13TeV-powheg-pythia8_TuneCUETP8M1/...
single top (s-ch)	10.32 (NLO) [10]	/ST_s-channel_4f_leptonDecays_13TeV-amcatnlo-pythia8_TuneCUETP8M1/...
$t\bar{t}$	831.8 (NLO) [10]	/TT_TuneCUETP8M2T4_13TeV-powheg-pythia8/...
$W(\to \ell\nu) + 0$ jets	49670.0 (NLO)	/WToLNu_0J_13TeV-amcatnloFXFX-pythia8/...
$W(\to \ell\nu) + 1$ jets	8264.0 (NLO)	/WToLNu_1J_13TeV-amcatnloFXFX-pythia8/...
$W(\to \ell\nu) + 2$ jets	2628.0 (NLO)	/WToLNu_2J_13TeV-amcatnloFXFX-pythia8/...
$Z/\gamma(\to \ell\ell)+$ jets (*)	5765.4 (NLO)	/DYJetsToLL_M-50_TuneCUETP8M1_13TeV-amcatnloFXFX-pythia8/...
$WW(\to \ell\nu)+$ jets	45.85 (NLO)	/WWTo1L1Nu2Q_13TeV_amcatnloFXFX_madspin_pythia8/...
$WW(\to 2\ell 2\nu)+$ jets	12.178 (NLO)	/WWTo2L2Nu_13TeV-powheg/
$WZ(\to \ell\nu)+$ jets	10.71 (NLO)	/WZTo1L1Nu2Q_13TeV_amcatnloFXFX_madspin_pythia8/...
$WZ(\to 2\ell 2\nu)+$ jets	5.595 (NLO)	/WZTo2L2Q_13TeV_amcatnloFXFX_madspin_pythia8/...
$ZZ(\to 2\ell 2\nu)+$ jets	3.22 (NLO)	/ZZTo2L2Q_13TeV_amcatnloFXFX_madspin_pythia8/...
μ-enriched QCD (**)	302672 (LO)	/QCD_Pt-20toInf_MuEnrichedPt15_TuneCUETP8M1_13TeV_pythia8/...

(b) (*) $m_{ll} > 50$ GeV; (**) $\hat{p}_T > 20$ GeV, $p_T^{\mu} > 15$ GeV

3.1 Object definition

In this section the basic analysis objects are defined on which the event selection and the kinematic reconstruction are based on. The candidates have been reconstructed with the particle-flow (PF) algorithm [14] which combines various subdetector information to perform a global particle type identification and momentum measurement.

3.1.1 Primary vertex

The reconstruction of tracks and primary vertices is detailed in Ref. [15]. If more than one primary vertex is identified, the one with largest sum of the squared transverse momenta of associated tracks is taken. Additionally, a "good" primary vertex candidate has to be fitted with ndof > 4 and reconstructed in the interaction region defined by $|d_z| < 24$ cm and $|d_{xy}| < 2$ cm with respect to the nominal interaction point.

3.1.2 Tight Muons

Events with exactly one muon within a pseudorapidity range of $|\eta| < 2.4$ and with a transverse momentum $p_{\mathrm{T}} > 26$ GeV are selected. The baseline muon selection contains "global muons" and has to meet additional muon quality requirements referred to as "tight muon ID" to select the most genuine muons from the PF muon collection.

More specifically, tight muons must have $\chi^2/\mathrm{ndof} < 10$ and at least one valid hit in the muon chambers, in order to suppress hadronic punch-through and muons from decays in flight. To guarantee a good p_{T} measurement, muon candidates are required to have more than 5 valid hits in the silicon tracker, out of which at least one in the pixel detector so as to further suppress muons from decays in flight. At least two muon chamber segments must match the global muon object to suppress punch-through and accidental track-to-segment matches. Furthermore, the transverse and longitudinal impact parameters must be smaller than $|d_{xy}| = 0.2$ cm and $|d_z| = 0.5$ cm with respect to the primary vertex in order to suppress muons from cosmic rays, muons from decays of long-lived hadrons (i.e. B, C hadrons), or from pileup interactions.

We define the "particle flow (relative) isolation" (I_{rel}) with the so-called "DeltaBeta" correction as

$$I_{\mathrm{rel}} = \frac{I^{\mathrm{ch.h}} + max((I^{\gamma} + I^{\mathrm{n.h}} - I^{\mathrm{PU}}), 0)}{p_{\mathrm{T}}}\,, \tag{2}$$

where $I^{\mathrm{ch.h}}$, I^{γ}, and $I^{\mathrm{n.h}}$ are the sum of the transverse energies deposited by stable particles like charged hadrons, photons and neutral hadrons respectively, in a cone of size $\Delta R = \sqrt{(\Delta\eta)^2 + (\Delta\phi)^2} = 0.4$ around the muon direction; $I^{\mathrm{PU}} \equiv \Delta\beta \times \sum p_T^{PU} \equiv 0.5 \times \sum p_T^{PU}$ is the sum of transverse momenta of tracks associated to non-leading, i.e. pileup, vertices, used to estimate the contribution of neutral particles from pileup events by applying a multiplicative factor of 0.5 that takes into account the neutral-to-charged particles ratio expected from isospin invariance. Therefore, the $\Delta\beta$ factor maps the expected neutral contribution in the isolation cone from the observed PU charged contribution. Tight muons are accepted by the requirement, which is expected to select signal events with $\sim 70\%$ efficiency The data-to-MC correction factors for muon are obtained using a "Tag and Probe" method and are applied to simulated events to account for differences in efficiencies between data and simulation. The correction factors for identification are provided by the muon object group while for isolation, as presented in Section 5.1, a similar method is used to exctract the numbers corresponding to $I_{\mathrm{rel}} < 0.06$ working point.

3.1.3 Tight Electrons

Events containing exactly one tight electron candidate are selected by requiring the presence of a "GsfElectron", i.e. an electron track fitted with the Gaussian-Sum-Filter that is matched to an active ECAL cell by the PF algorithm, with $E_{\mathrm{T}} > 35$ GeV, $|\eta| < 2.1$ while excluding the ECAL barrel-endcap transition region of $1.44 < |\eta| < 1.57$. Additional quality criteria are applied based on nine variables through an optimized cut-based approach. Due to the presence of strong correlation between the $\Delta\phi$ and $|1/E - 1/p|$ (with E the ECAL supercluster energy and p the track momentum at the point of closest approach to the beam spot) variables, optimization has been achieved only for one of them, albeit making a reasonable cut for the other. The analyses make use of the "tight" working point yielding an efficiency of 80–90% for electrons above 45 GeV.

3.1.4 Veto of additional muons or electrons

Events containing additional muons or electrons besides either one tight muon or electron candidate are vetoed. This reduces the contamination by Z+jets and dileptonic $\mathrm{t\bar{t}}$ background events. The selection requirements for these additional leptons are loosened with respected to the tight criteria.

Loose muons are required to fall within $|\eta| < 2.4$ while having $p_{\mathrm{T}} > 10$ GeV and being reconstructed as "global" or "tracker" muon together with a relative isolation of $I_{\mathrm{rel}} < 0.2$. Loose electron candidate have to pass a cut-based quality selection similar to the tight electron selection defined above whereas the kinematic requirements are $E_{\mathrm{T}} > 15$ GeV, $|\eta| < 2.5$. The selection chain for electron identification used for such electrons is tuned to have a higher efficiency, thus resulting in a tighter cut on the veto. The present analysis then makes use of the cut-based "electron veto" working point yielding an efficiency of 98% at a plateau which is reached around $E_{\mathrm{T}} > 45$ GeV.

3.1.5 Jets

Jets are clustered from PF candidate using the anti-k_t clustering algorithm [16] with a cone size of $R = 0.4$. The influence of pileup is mitigated using the charged hadron subtraction technique (CHS) [17] in which PF candidates not associated to the primary vertex are ignored in the clustering. A potential overlap of jets with a selected tight muon or electron is omitted by ignoring jets which are closer than $\Delta R = 0.4$ with respect to tight muon or electron candidate.

The resulting jets have the standard multi-level jet energy corrections (JEC) applied (L1FastJet, L2, L3). Technically, we apply the `Summer16v4` corrections determined from simulation on both data and simulation. For data we further apply residual corrections derived from data themselves. Furthermore the jet energy resolution (JER) is corrected in simulation to match the one observed in data by smearing the jet energy using dedicated scale factors. The analysis considers jets within $|\eta| < 4.7$ whose calibrated transverse energy is greater than 40 GeV and which pass a set of loose quality cuts which are detailed in the following. The cuts are different depending on the pseudorapidity of the jets as different PF information are available.

- For PF jets with $|\eta| < 2.7$, neutral hadronic and neutral electro-magnetic energy fractions must be smaller than 99% and more than one constituent must be present. Additionally, for PF jets with $|\eta| < 2.4$ the number of charged hadrons and the respective energy fraction must be greater than 0, and the charged electro-magnetic energy fraction must be smaller than 99%.
- For PF jets with $2.7 < |\eta| < 3.0$ the definition is different: the neutral electro-

magnetic energy fraction is required to be greater than 0.01 and the neutral hadron fraction must be smaller than 98%, while the number of neutral particles must be greater than 2.

- Finally, for PF jets with $|\eta| > 3.0$ neutral electro-magnetic energy fraction must be $< 90\%$ and the number of neutral particles greater than 10.

3.1.6 b Tagging

Several b-tagging, i.e. identification of jets originating from b quarks, algorithms are available in CMS. Some exploit the long B-hadrons lifetime, others their semi-leptonic decay modes and others use kinematic variables related to the high B-meson mass and hard b-quark fragmentation function. Details are provided elsewhere [18]. More specifically, b-tagging algorithms are based on displaced tracks (track counting taggers, jet probability tagger), the presence of "secondary" vertices (secondary vertex taggers) or soft leptons (soft lepton taggers) or on a combination of these (combined secondary vertex taggers). The combined secondary vertex algorithm uses track-based lifetime information together with secondary vertices inside the jet to provide a MVA discriminator for b jet identification (Combined MVA v2) [19]. For this study we use the CMVAv2 algorithm at the "tight" working point corresponding to a threshold set to 0.9432 and a 0.1% gdus mistag efficiency—estimated based on simulated jets with $p_{\mathrm{T}} > 60\,\mathrm{GeV}$—as recomeneded by the b-tagging Physics Object Group (POG) [20].

3.1.7 Missing transverse energy

Defined in an analogous way as PF-based jets, PF-based $\not\!\!E_{\mathrm{T}}$ is the opposite of the vectorial sum of the transverse momenta of the identified PF particles

$$\not\!\!E_{\mathrm{T}}^{\mathrm{raw}} = |\vec{\not\!\!p}_{\mathrm{T}}^{\,\mathrm{raw}}| = \Big| - \sum_{i}^{\text{all PF}} \vec{p}_i \Big| \,. \tag{3}$$

The $\not\!\!E_{\mathrm{T}}$ receives corrections (type I) by propagating the vectorial difference between uncalibrated and calibrated jets (only L2 and L3) to the $\not\!\!E_{\mathrm{T}}$. The correction can be expressed as

$$\vec{\not\!\!p}_{\mathrm{T}}^{\,\mathrm{corr.}} = - \sum_{i}^{\text{unclustered}} \vec{p}_i \; - \sum_{i}^{\text{jets}} \vec{p}_i^{\,\mathrm{corr.}} \tag{4}$$

$$= \vec{\not\!\!p}_{\mathrm{T}}^{\,\mathrm{raw}} + \sum_{i}^{\text{jets}} \left(\vec{p}_i^{\,\mathrm{L123}} - \vec{p}_i^{\,\mathrm{L1}} \right) , \tag{5}$$

which yields an improved $\not\!\!E_{\mathrm{T}}$ energy scale and resolution [21].

3.2 High level trigger selection

At high level trigger, in the muon channel events are selected if they pass the `HLT_IsoMu24` OR the `HLT_IsoTkMu24` path where the presence of an isolated online muon candidate with $p_{\mathrm{T}} > 24$ GeV is required. Efficiencies for this trigger in simulation are corrected using data-to-MC correction factors obtained from a "Tag and Probe" method. In the electron channel events need to pass the trigger path `HLT_Ele32_eta2p1_WPTight_Gsf_vX`, where the online electron is restricted to have $p_{\mathrm{T}} > 32$ GeV and $|\eta| < 2.1$. The respective trigger correction factors were not provided by the E/gamma Physics Object Group and have been hence calculated as detailed in Sec. 5.2.3

3.3 Signal and control regions

The signature of the t-channel single-top production includes one light quark recoiling against the virtual W boson, one b quark from the top-quark decay, and a second b quark from the initial gluon splitting.

The second b quark has a softer p_{T} and a harder η spectrum with respect to the one coming from the top-quark decay. As a result, jets stemming from the hadronization of the latter are less likely to be selected due to the p_{T} cut on the jet, and if selected they are less likely to be tagged, due to the intrinsic limit on the acceptance in η of the b-tagging algorithm, which is limited to the tracker acceptance ($|\eta| < 2.4$). For that reason the region with two jets, with one of them being tagged as b jet, provides the largest fraction of signal events. In order to test the modelling of the main background processes it is useful to define further regions, which are enriched in certain background processes. For that purpose we use the notation "nJmT" or the wording "n-jets, m-tags" to refer to a sample that has exactly n reconstructed jets, exactly m of which pass the b tag threshold. Notable samples which are studied and used in this analysis are the 2J0T sample (enriched in W+jets), the 2J1T sample (signal region with the largest signal fraction among all regions), and the 3J2T region (enriched in $\mathrm{t\bar{t}}$).

3.4 Transverse W boson mass

To further suppress contributions from processes where the muon does not come from a leptonically decaying W boson, a selection based the reconstructed transverse W-boson mass $m_{\mathrm{T}}^{\mathrm{W}}$ can be applied. It is defined as

$$m_{\mathrm{T}}^{\mathrm{W}} = \sqrt{(p_{T,l} + p_{T,\nu})^2 - (p_{x,l} + p_{x,\nu})^2 - (p_{y,l} + p_{y,\nu})^2}\,, \tag{6}$$

where the transverse momentum of the neutrino is approximated by the missing transverse energy vector, $\vec{\not{p}}_{\mathrm{T}}$.

4 Top quark reconstruction

In order to analyze the kinematics of singly produced top quarks, the fourvector of the top quarks have to be reconstructed from the decay products. All top-quark decay products are reconstructed in the detector, except for the neutrino which escapes unobserved. While the transverse momentum of the neutrino can be inferred from the missing transverse energy, its longitudinal momentum has to be derived based on extra assumptions. Once the leptonically decaying W boson is reconstructed the selected jets have to be assigned to the final state quarks in the top quark decay chain.

4.0.1 W-boson reconstruction

The first step in the reconstruction of the top quark from its decay products is the reconstruction of the W boson. We assume that the x and y components of the missing transverse energy are entirely due to the escaping neutrino, and apply the W-mass constraint in order to extract the unknown z component ($p_{z,\nu}$):

$$m_{\mathrm{W}}^2 = (E_\ell + \sqrt{\not{E}_{\mathrm{T}}{}^2 + p_{z,\nu}^2})^2 - (\vec{p}_{T,\ell} + \vec{\not{p}}_{\mathrm{T}})^2 - (p_{z,\ell} + p_{z,\nu})^2\,. \tag{7}$$

This equation has in general two solutions:

$$p_{z,\nu} = \frac{\Lambda \cdot p_{z,\ell}}{p_{T,\ell}^2} \pm \sqrt{\frac{\Lambda^2 \cdot p_{z,\ell}^2}{p_{T,\ell}^4} - \frac{E_\ell^2 \cdot \not{E}_{\mathrm{T}}{}^2 - \Lambda^2}{p_{T,\ell}^2}}\,, \tag{8}$$

with

$$\Lambda = \frac{m_{\mathrm{W}}^2}{2} + \vec{p}_{T,\ell} \cdot \vec{\not{p}}_{\mathrm{T}}\,. \tag{9}$$

In the case of two real solutions for $p_{z,\nu}$ (in 65% of all cases), different choice criteria have been proposed [22, 23]. The solution with the smallest absolute value is chosen in the present analysis. By looking at truth information in simulated events it is found that, in 63.4% of the selected events with real solutions, the smallest $|p_{z,\nu}|$ solution is closer to the true neutrino p_z than the other solution.

If the discriminant in Eq. (8) becomes negative, or equivalently $m_{\mathrm{T}}^{\mathrm{W}}$ is larger than m_{W}, the solutions have an imaginary component. This happens in 35% of the cases, mostly due the finite $\not{E}_{\mathrm{T}}$ resolution. Lepton momentum resolution and the finite W intrinsic width give negligible contributions. Several schemes have been used to deal with this situation [22, 23]. In this analysis the imaginary component is eliminated by modifying $\not{E}_{\mathrm{T}}$ such to give $m_{\mathrm{T}}^{\mathrm{W}} = m_{\mathrm{W}}$, still respecting the m_{W} constraing from Eq. (7). This is obtained by imposing that the discriminator, and thus the square-root term in Eq. (8), are null. This condition gives a quadratic relation between $p_{x,\nu}$ and $p_{y,\nu}$, with two possible solutions, among which the one with minimal distance between $p_{T,\nu}$ and $\not{E}_{\mathrm{T}}$ is chosen.

4.0.2 Jet-parton assignment

In the second step the selected jets have to be assigned to the final state quarks from the top-quark decay. In the 2J1T region the procedure is straight forward: the tagged jet is assigned to the b-quark from the top-quark decay, the non-tagged jet is assigned to the light quark. The b-tagged jet matches the true b quark from top-quark decay in simulated events in about 83.9% of the selected signal events, using as matching criterion a distance of $\Delta R < 0.3$ between the jet and the parton. The fraction of events with wrong assignmet are events in which the selected b-tagged jet stems from the second b-quark from the initial gluon splitting and not from the decay of the top quark.

In the 3J2T region the non-tagged jet is again assigned to the light quark. From the two tagged jets the one with the larger value of the b-tag discriminator is assigned to the b quark from the top-quark decay, while the other tagged jet is assigned to the second b quark from the gluon splitting. This choice is correct in 48.4% of all cases, estimated on simulated signal events using the same matching criterion as described above.

5 Trigger and lepton efficiencies

5.1 Muon identification, isolation and trigger efficiencies

Muon trigger, identification and isolation efficiencies for the full 2016 dataset, listed in Tab. 1, are provided centrally (default isolation criterion 0.15) by the Muon Physics Object Group [24]. As we use a tighter isolation criterion (0.06) than the default one, we need to re-calculate the identification, isolation and trigger efficiencies on our own, and these will be applied as weights to the MC samples.

Table 2: MC sample used for the muon efficiency measurement. MC sample used has been corrected for the pileup effects for the efficiency extraction.

Sample	Sample Name
Drell-Yann	/DYJetsToLL_M-50_TuneCUETP8M1_13TeV-madgraphMLM-pythia8/..

Muon efficiencies are calculated using the official Tag and Probe tool provided by the Muon Physics Object Group [25] which utilizes the known resonances, e.g. J/ψ, Z, to measure object efficiencies. In the tag-probe method, "tagged" muon is required to pass a very tight selection where as the "probe" muon is required to pass a loose selection as compared to the tagged muon. The "tag-and-probe" pair is selected such that the invariant mass of tag-and-probe falls within the selected mass resonance window. The efficiency ($\epsilon = N_{passing}/N_{passing+failing}$) in-turn for the data and MC is extracted by fiting the resonance peak. The data to MC simulation scale factors (SF) are than derived as SFs = $\epsilon^{Data}/\epsilon^{MC}$. The Muon efficiencies are extracted using the full 2016 dataset listed in Tab. 1 and for the MC simulation Drell-Yan process listed in Tab. 3, generated with MadGraph_aMC@NLO are used. The muon efficiency results are approved later by Muon Physics Object Group [26].

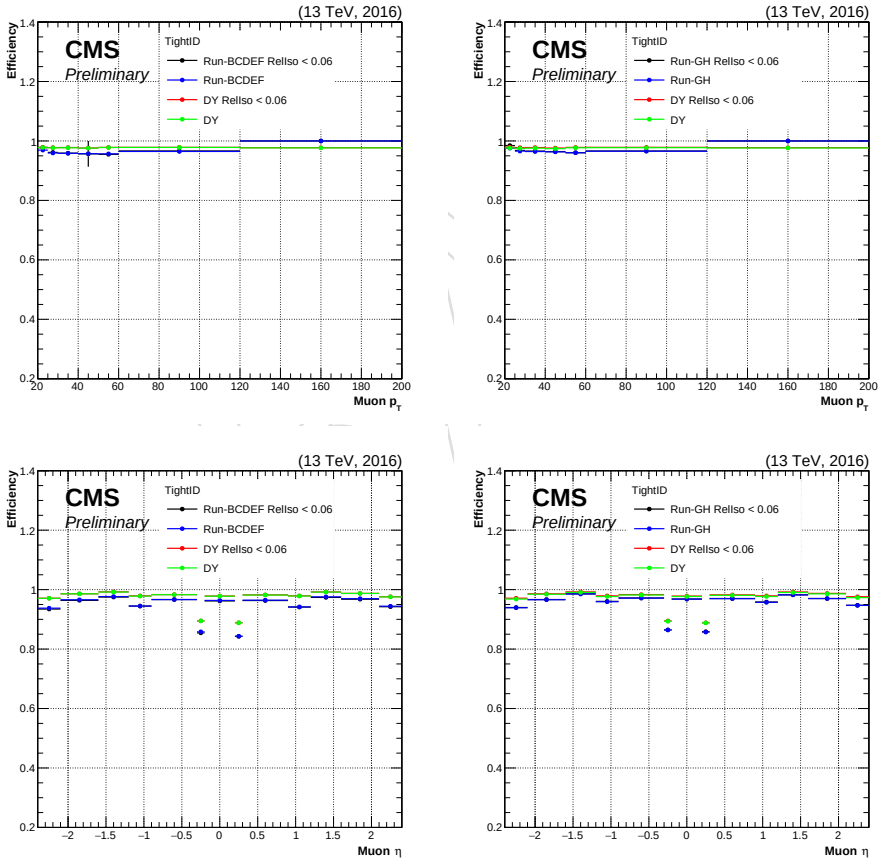

Figure 2: Muon tight ID efficiency in bins of p_T and η for Run-BCDEF and Run-GH for $I_{rel} < 0.06$ superposed with tight ID efficiency with $I_{rel} < 0.20$. The legend entries with black(red) shows efficiencies in data(MC) for $I_{rel} < 0.06$ as compared to blue(green) for $I_{rel} < 0.15$ from Muon POG.

The muon tight ID and reconstruction efficiencies are re-evaluated for the Run-BCDEF and Run-GH on the same lines as the centrally produced identification and reconstruction efficien-

cies by the Muon POG for the side by side comparison of muon efficiencies produced for tight isolation (0.06) and loose isolation (0.15). For the tight ID the tagged muon has to pass the tight identification criterion, i.e., the candidate selected has to pass the trigger segment `IsoMu24 || IsoTkMu24`, $p_T > 26$ GeV, is reconstructed as a Global Muon, the candidate has to be a PF muon, muon segments reconstructed in at least two stations, χ^2 requirements on track, combines track and chamber hits, muon segments reconstructed in at least two stations, tag-probe pair multiplicity has to be always one, has to pass impact parameter cut, at least one pixel hit and the $\Delta R(tag, probe)$ >0.3. The tagged object is a general tracker muon with p_T >20 GeV. On top of tight identification requirement, the "particle flow (relative) isolation" with "Delta-Beta" correction has to be $I_{rel} < 0.06$. Finally, the signal component is obtained by fitting the $70 < mass(\mu^+\mu^-) < 130$ GeV and the background component is obtained by fitting with a sum of two Voigtians. Figure 2 shows the muon ID efficiency in bins of p_T and η for different run ranges, with tight and loose isolation working points super-imposed. The impact of tight isolation working point on the muon identification efficiency is very small with respect to the ID efficiencies due to the loose isolation working point.

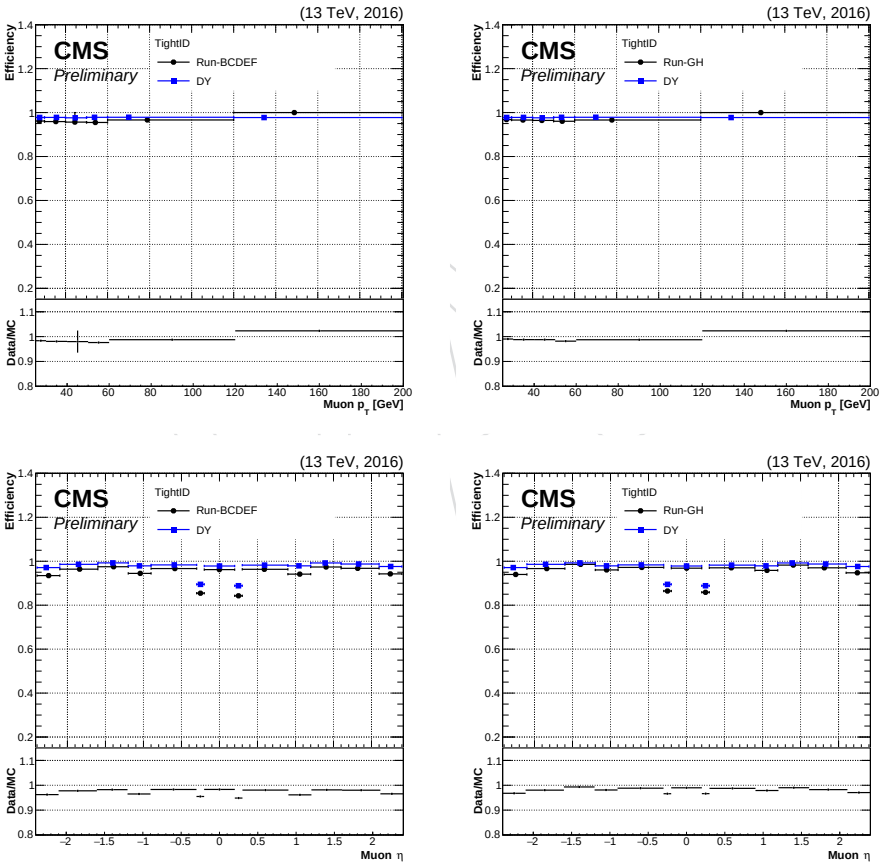

Figure 3: Muon tight ID efficiency in bins of p_T and η for Run-BCDEF, Run-GH and data for $I_{rel} < 0.06$.

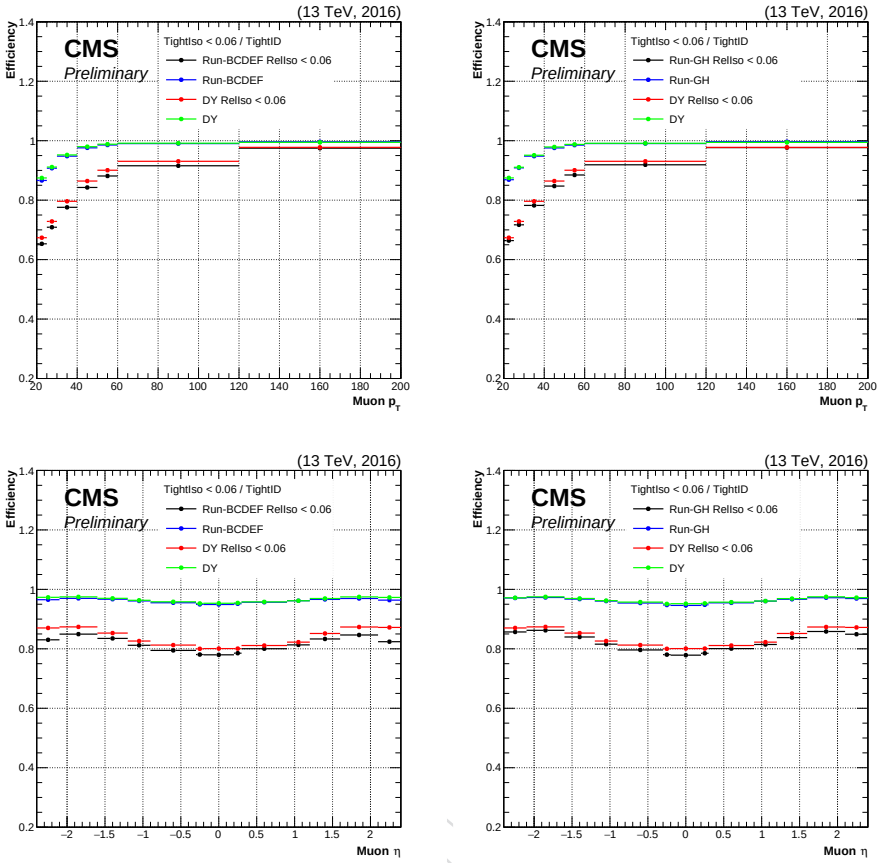

Figure 4: Muon tight isolation efficiency in bins of p_{T} and η for Run-BCDEF and Run-GH for $I_{\mathrm{rel}} < 0.06$ super imposed with tight ID efficiency with $I_{\mathrm{rel}} < 0.15$ from Muon POG.

Muon isolation efficiencies for the tight(loose) working points 0.06(0.15) are extracted for the Run-BCDEF, GH and are shown in Fig. 4. The drop in efficiency is due to the choice of isolation working point. To understand the drop in the efficiency for tight isolation working point, a comparison with the centrally produced isolation efficiencies from Muon POG is made by changing the tight isolation working point back to 0.15 from 0.06 and reproducing the efficiencies for 0.15. The comparison between the two is shown in the Fig 6.

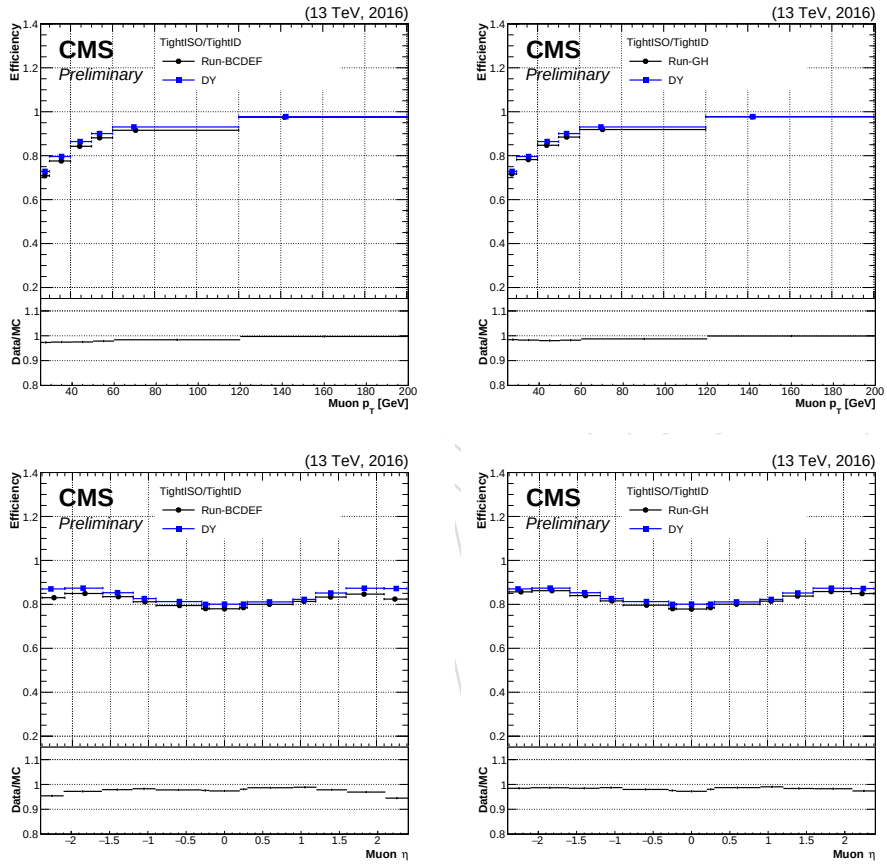

Figure 5: Muon tight isolation efficiency in bins of p_{T} and η for Run-BCDEF, Run-GH and data for $I_{\mathrm{rel}} < 0.06$.

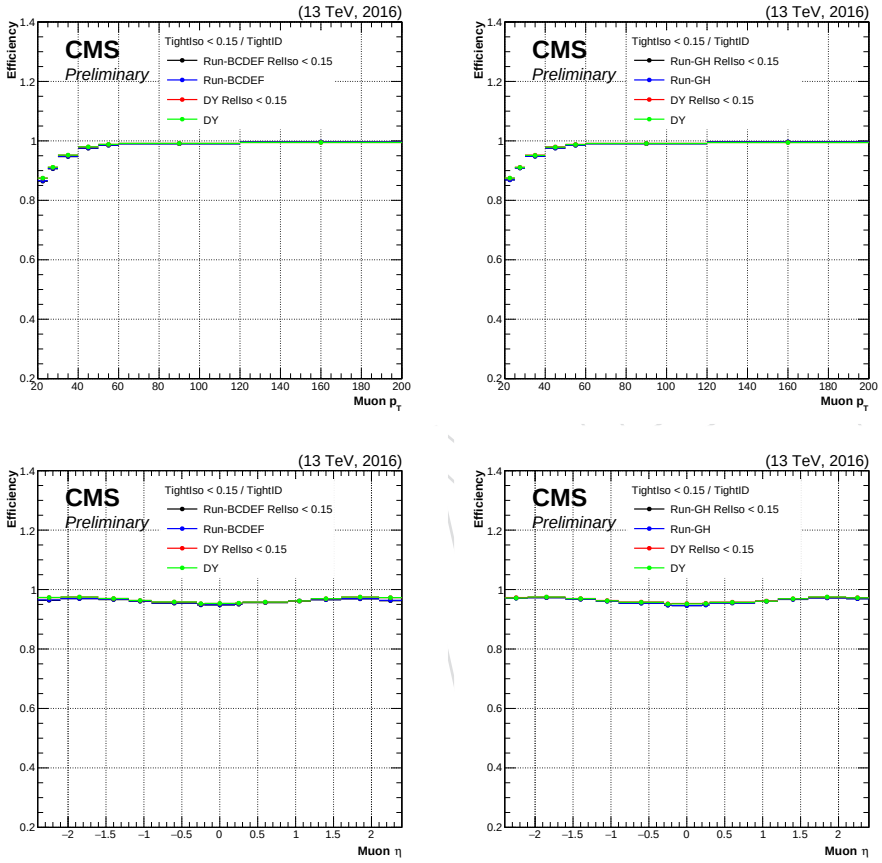

Figure 6: Muon isolation efficiency in bins of p_{T} and η for Run-BCDEF and Run-GH for $I_{\mathrm{rel}} < 0.15$ superposed with Muon POG extracted isolation efficiencies.

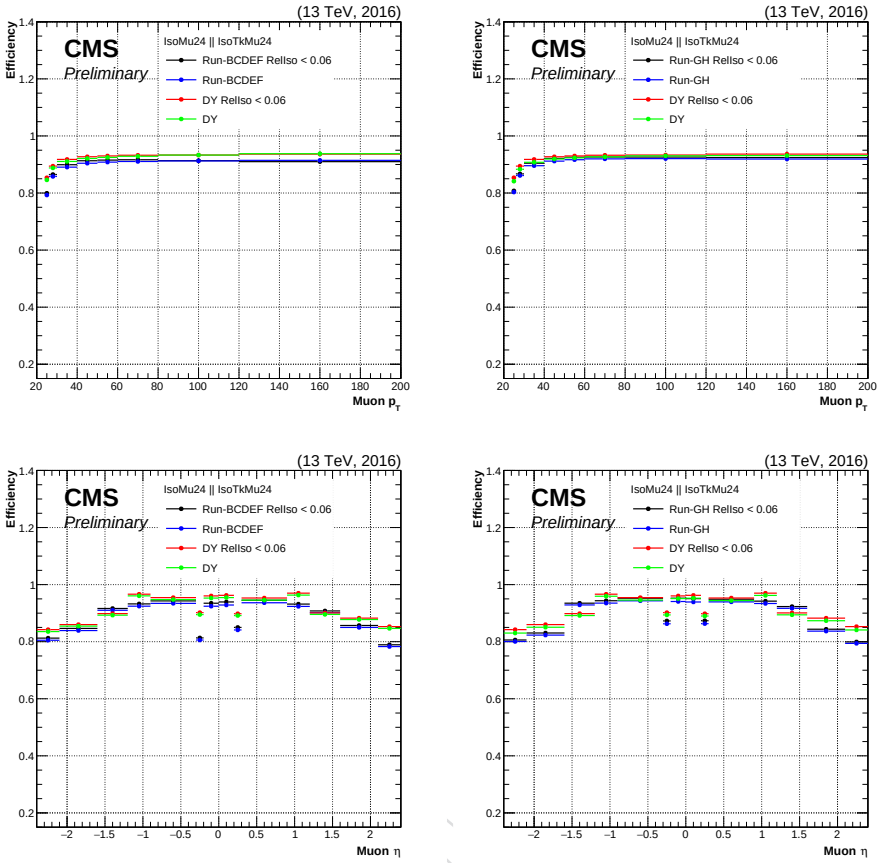

Figure 7: Muon trigger efficiency in bins of p_T and η for Run-BCDEF and Run-GH for $I_{rel} < 0.06$ superposed with trigger efficiency with $I_{rel} < 0.15$ from Muon POG.

The efficiency of `HLT_IsoMu24 or HLT_IsoTkMu24` is measured, such that the tagged muon is required to pass the tight identification on top of isolation criterion and matched with HLT muon objects. The probe muons are required to match with trigger bits. Figure 7 shows the muon trigger efficiency in the bins of p_T and η for the data and MC simulations, the muon trigger efficiency with loose working point (0.15) are super imposed for a comparison. On top of statistical uncertainties, systematics uncertainties studied with respect to the nominal are: varying the shape of fitting function from sum of two Voigtians to a single Voigtians, changing the Z-mass window from 130 GeV to 120 GeV keeping the lower edge fixed to 70 GeV and by varying the isolation working point up/down (0.08/0.04) from its nominal value 0.06. The overall impact of these additional systematics w.r.t to the nominal added in quadrature is around 1.3%, details are listed in Tab. 3.

Table 3: Systematic uncertainties due the shape of fitting function, Z-mass window and isolation in addition to the statistical uncertainties.

Variable	Data	SF $\pm$ stat.	Δ(mass)%	Δ(shape)%	Δ(iso.)%	Total(%)
Trigger	BCDEF	0.97 ± 0.01	0.05	0.09	0.03	0.10
	GH	0.98 ± 0.01	0.03	0.05	0.04	0.07
ID	BCDEF	0.98 ± 0.01	0.09	0.70	0.00	0.70
	GH	0.99 ± 0.01	0.30	0.53	0.00	0.60
ISO	BCDEF	0.98 ± 0.00	0.35	0.05	0.76	0.83
	GH	0.99 ± 0.00	0.01	0.01	0.44	0.44

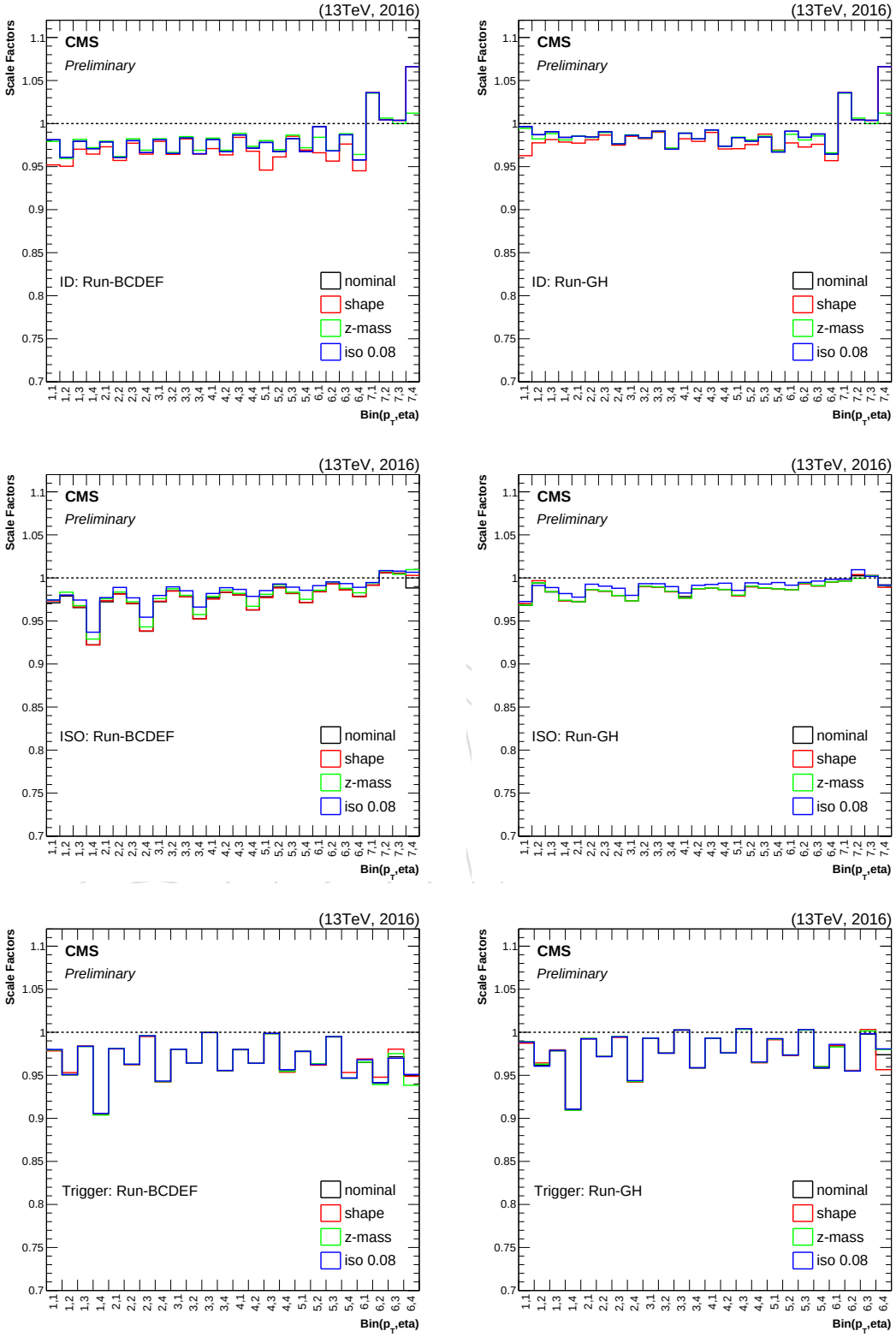

Figure 8: Variations of scale factors for ID, isolation, and trigger with respect to the nominal for the Run-BCDEF and Run-GH.

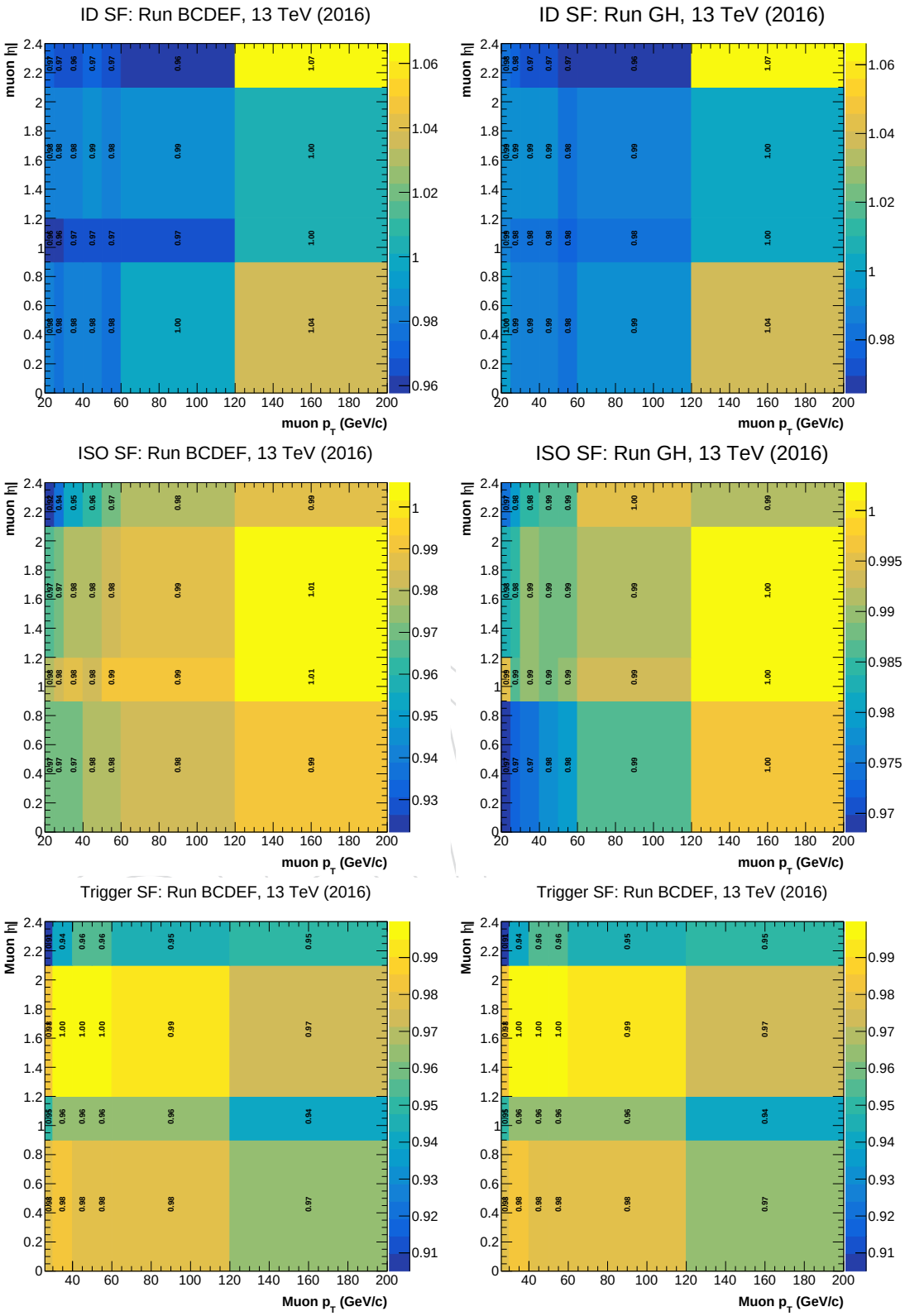

Figure 9: Scale factors for ID, isolation and trigger in bins of η vs p_{T} for the Run-BCDEF and Run-GH.

5.2 Electron trigger, reconstruction, ID, isolation efficiencies

5.2.1 Electron ID and reconstruction efficiencies

Since the cut-based "electron tight" and "electron veto" working points are being used in the analysis, the ID scale factors will be applied as weights to the MC samples for the individual electrons, as well as the respective reconstruction efficiencies. The scale factors are provided by the E/gamma Physics Object Group [27].

5.2.2 Electron isolation efficiencies

The isolation itself is part of the cutflow used for the different cut-based electron WPs [28], leaving no need to apply further isolation efficiencies.

5.2.3 Electron trigger efficiencies

Electron trigger efficiencies and scale factors (SFs) for the High-Level-Trigger (HLT) `HLT_Ele32_eta2p1_WPTight_Gsf` were calculated using the official Tag and Probe tool provided by the E/gamma Physics Object Group [29] and were approved by the latter in the Joint ECAL DPG/EGM POG meeting [30]. The efficiency to select events with electrons having an HLT match was estimated using a well known resonance decaying in the dileptonic channel, i.e. the decay of a Z boson to two oppositely charged electrons. To select events with this topology, an electron called "tag" passing tight selection criteria (Tab. 4) is required. In addition, an oppositely charged electron called "probe" passing looser criteria is necessary. The invariant mass of the dilepton-pair is restricted to be between $60 < m_{e^+e^-} < 120\,\text{GeV}$. Splitting the probes into collections, where one contains electrons with an HLT match, i.e. the "passing probes", and one containing electrons without an HLT match, i.e. the "failing probes", allows to estimate the efficiency by dividing the amount of passing probes to the total number of probes

$$\varepsilon = \frac{N_{\text{passing}}}{N_{\text{passing}} + N_{\text{failing}}}. \tag{10}$$

The SFs were hence calculated by dividing the efficiency estimated in data to the efficiency estimated in simulation

$$SF = \frac{\varepsilon_{\text{Data}}}{\varepsilon_{\text{MC}}}. \tag{11}$$

Because of the tight cut-based ID applied for both tags and probes, the contamination with background is negligible, hence simply allowing the SFs to be measured using a cut-and-count approach.

At the end of data taking in 2016 most of the Level-1-Trigger (L1T) seeds were prescaled. This evolution of L1T prescales leads to a bias in the efficiency measurement. The lowest-p_T unprescaled L1T that was enabled during the whole year is `L1_SingleIsoEG34er`. To perform an unbiased calculation, in addition to the HLT match, a `L1_SingleIsoEG34er` match for the tag was demanded. The L1T match was applied by looping over all L1T objects with $E_T > 34$ GeV, $|\eta| < 2.131$ and l1t::EGamma::hwIso() ≥ 1 [31] around the tag in a cone of size $\Delta R = 0.3$. If multiple L1T objects were found, the one with the highest E_T was chosen and if no object was found, the tag and probe pair was rejected. In order to be on the plateau of this trigger, the transverse momentum of the tag was set to be greater than 40 GeV.

In the following section, the results of the SF measurement are mapped. They were calculated for transverse momenta $30 < p_T < 500\,\text{GeV}$, starting with a broader binning at $p_T > 56$ GeV. The supercluster-eta range corresponds to values $|\eta_{SC}| < 2.1$.

Table 4: List of the selection criteria applied on tags and probes. Tags are required to pass tighter selection criteria, visible in the minimum transverse momentum $p_T > 40\,\text{GeV}$, the tight cut-based ID, the impact parameter cuts [28] and the HLT and L1T matches. Additional, tags stemming from the transition gap between barrel and endcap corresponding to supercluster-eta values $1.4442 < |\eta_{SC}| < 1.566$ are being rejected.

Selection	Tag	Probe
Min p_T (GeV)	40	25
$\lvert\eta_{SC}\rvert$	< 2.1	< 2.1
Tight cut-based ID	✓	✓
IP cuts	✓	✓
Exclude endcap-barrel-gap	✓	x
HLT match	✓	x
L1T match	✓	x

Figure 10 shows both efficiencies for data and MC and the corresponding distribution of the SF in dependence of the transverse momentum of the probe restricted to values between $25 < p_T < 200\,\text{GeV}$ and using the full probe-eta range. A large turn-on behavior of the HLT under study is observed, reaching the plateau of the trigger at high p_T values. As described in 3.1.3 only electrons with $p_T > 35$ GeV are being considered in the analysis, corresponding to SFs very close to one.

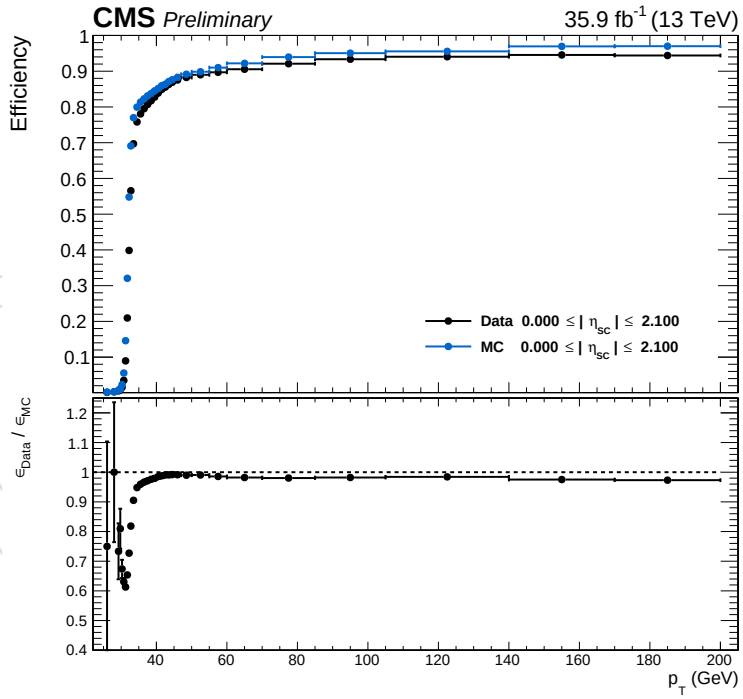

Figure 10: Distribution of the efficiencies in data and MC and the corresponding SF in dependence of the transverse momentum of the probe using the full probe-eta range.

The measured SFs with respect to $30 < p_T < 200$ GeV and $|\eta_{SC}| < 2.1$ are displayed in figure 11 (a). In the analysis electrons stemming from the transition gap between barrel and endcap are being rejected. In most of the phase space the SFs reach values close to one. Figure 11 (b) shows the combined uncertainty composed of the statistical uncertainty and two systematic shifts. The first shift is introduced by changing the criteria for the dilepton mass from the original restriction $60 < m_{e^+e^-} < 120\,\text{GeV}$ to $70 < m_{e^+e^-} < 110\,\text{GeV}$. The absolute difference for the SFs arising through this procedure is taken into account. In the same way the second shift is estimated by changing the minimum transverse momentum of the tag from $p_T > 40$ GeV to $p_T > 45$ GeV. The combined uncertainty is hence calculated using the sum in quadrature and reaches values of roughly ≤ 0.02 in the barrel and ≤ 0.03 in the endcap region.

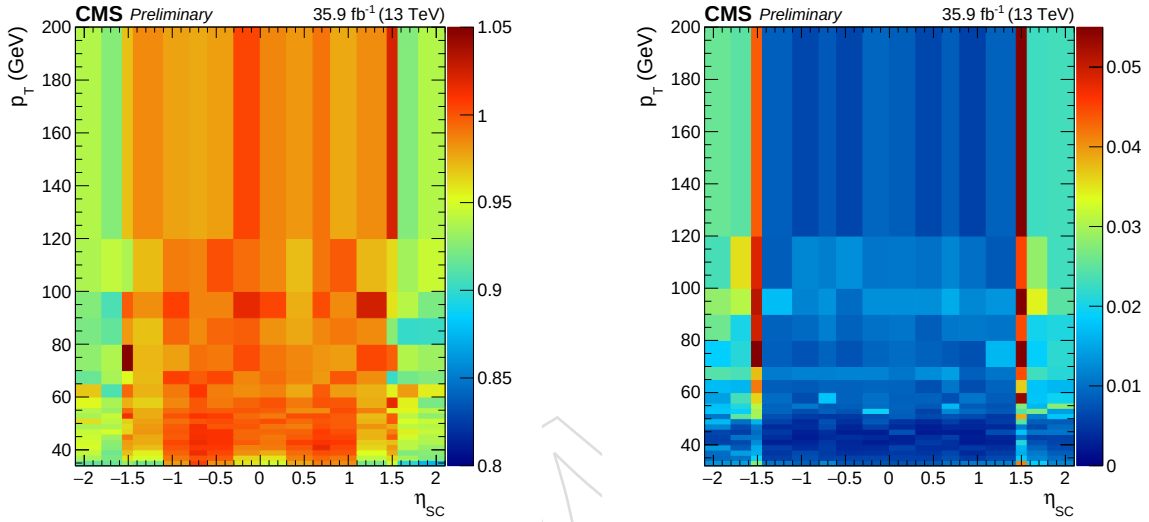

(a) (b)

Figure 11: Two dimensional plots with respect to p_T and η_{SC} showing the calculated scale factors on the z-axis in (a) and the combined uncertainty on the z-axis in (b) composed of the statistical uncertainty and two systematic shifts. The combined uncertainty is calculated using the sum in quadrature.

References

[1] E. Re, "Single-top Wt-channel production matched with parton showers using the POWHEG method", *Eur. Phys. J.* **C71** (2011) 1547, doi:10.1140/epjc/s10052-011-1547-z, arXiv:1009.2450.

[2] S. Alioli, P. Nason, C. Oleari, and E. Re, "A general framework for implementing NLO calculations in shower Monte Carlo programs: the POWHEG BOX", *JHEP* **06** (2010) 043, doi:10.1007/JHEP06(2010)043, arXiv:1002.2581.

[3] S. Alioli, P. Nason, C. Oleari, and E. Re, "NLO single-top production matched with shower in POWHEG: s- and t-channel contributions", *JHEP* **09** (2009) 111, doi:10.1088/1126-6708/2009/09/111, arXiv:0907.4076.

[4] S. Frixione, P. Nason, and C. Oleari, "Matching NLO QCD computations with Parton Shower simulations: the POWHEG method", *JHEP* **0711** (2007) 070, doi:10.1088/1126-6708/2007/11/070, arXiv:0709.2092.

[5] T. Sjöstrand, S. Mrenna, and P. Skands, "PYTHIA 6.4 physics and manual", *JHEP* **05** (2006) 026, doi:10.1088/1126-6708/2006/05/026, arXiv:hep-ph/0603175.

[6] P. Skands, S. Carrazza, and J. Rojo, "Tuning PYTHIA 8.1: the Monash 2013 Tune", *Eur. Phys. J.* **C74** (2014), no. 8, 3024, doi:10.1140/epjc/s10052-014-3024-y, arXiv:1404.5630.

[7] R. Frederix and S. Frixione, "Merging meets matching in MC@NLO", *JHEP* **12** (2012) 061, doi:10.1007/JHEP12(2012)061, arXiv:1209.6215.

[8] *https://twiki.cern.ch/twiki/bin/view/CMSPublic/WorkBookMiniAOD*.

[9] *https://cms-service-dqm.web.cern.ch/cms-service-dqm/CAF/certification/*.

[10] TOPLHCWG, "Nlo single-top t channel cross sections", *https://twiki.cern.ch/twiki/bin/view/LHCPhysics/SingleTopRefXsec*.

[11] N. Kidonakis, "Differential and total cross sections for top pair and single top production", arXiv:1205.3453.

[12] M. Aliev et al., "Hathor - hadronic top and heavy quarks cross section calculator", arXiv:1007.1327.

[13] J. Allison et al., "Geant4 developments and applications", *IEEE Transactions on Nuclear Science* **53, 1** (2006) 270–278.

[14] CMS Collaboration, "Particle–flow event reconstruction in CMS and performance for jets, taus, and $\not\!\!E_{\mathrm{T}}$", CMS Physics Analysis Summary CMS-PAS-PFT-09-001, 2009.

[15] CMS Collaboration, "Description and performance of track and primary-vertex reconstruction with the CMS tracker", *JINST* **9** (2014), no. 10, P10009, doi:10.1088/1748-0221/9/10/P10009, arXiv:1405.6569.

[16] M. Cacciari, G. P. Salam, and G. Soyez, "The anti-k_t jet clustering algorithm", *JHEP* **04** (2008) 063, doi:10.1088/1126-6708/2008/04/063, arXiv:0802.1189.

[17] CMS Collaboration, "Pileup Removal Algorithms", CMS Physics Analysis Summary CMS-PAS-JME-14-001, 2014.

[18] T. C. collaboration, "Identification of b-quark jets with the cms experiment", *Journal of Instrumentation* **8** (2013), no. 04, P04013.

[19] CMS Collaboration, "Identification of b quark jets at the CMS Experiment in the LHC Run 2", CMS Physics Analysis Summary CMS-PAS-BTV-15-001, 2016.

[20] *https://twiki.cern.ch/twiki/bin/viewauth/CMS/BtagRecommendation80XReReco*.

[21] CMS Collaboration, "Performance of missing energy reconstruction in 13 TeV pp collision data using the CMS detector", CMS Physics Analysis Summary CMS-PAS-JME-16-004, 2016.

[22] D0 Collaboration, "Observation of Single Top-Quark Production", *Phys. Rev. Lett.* **103** (2009) 092001, doi:10.1103/PhysRevLett.103.092001, arXiv:0903.0850.

[23] CDF Collaboration, "First Observation of Electroweak Single Top Quark Production", *Phys. Rev. Lett.* **103** (2009) 092002, doi:10.1103/PhysRevLett.103.092002, arXiv:0903.0885.

[24] *https://twiki.cern.ch/twiki/bin/view/CMS/MuonWorkInProgressAndPagResults*.

[25] *https://twiki.cern.ch/twiki/bin/viewauth/CMS/MuonTagAndProbeTreesRun2*.

[26] *https://indico.cern.ch/event/670008*.

[27] *https://twiki.cern.ch/twiki/bin/view/CMS/EgammaIDRecipesRun2*.

[28] *https://twiki.cern.ch/twiki/bin/viewauth/CMS/CutBasedElectronIdentificationRun2*.

[29] *https://twiki.cern.ch/twiki/bin/view/CMSPublic/ElectronTagAndProbe*.

[30] *https://indico.cern.ch/event/604950/*.

[31] *https://twiki.cern.ch/twiki/pub/CMS/GlobalTriggerMenu_L1Menu_Collisions2016_v10/L1Menu_Collisions2016_v10.html#L1_SingleIsoEG34er*.